ADVANCED FUNCTIONAL MATERIALS
www.afm-journal.de

Collectively Exhaustive Electrodes Based on Covalent Organic Framework and Antagonistic Co-Doping for Electroactive Ionic Artificial Muscles

*Sandipan Roy, Jaehwan Kim, Moumita Kotal, Rassoul Tabassian, Kwang J. Kim, and Il-Kwon Oh**

In this study, high-performance ionic soft actuators are developed for the first time using collectively exhaustive boron and sulfur co-doped porous carbon electrodes (BS-COF-Cs), derived from thiophene-based boronate-linked covalent organic framework (T-COF) as a template. The one-electron deficiency of boron compared to carbon leads to the generation of hole charge carriers, while sulfur, owing to its high electron density, creates electron carriers in BS-COF-C electrodes. This antagonistic functionality of BS-COF-C electrodes assists the charge-transfer rate, leading to fast charge separation in the developed ionic soft actuator under alternating current input signals. Furthermore, the hierarchical porosity, high surface area, and synergistic effect of co-doping of the BS-COF-Cs play crucial roles in offering effective interaction of BS-COF-Cs with poly(3,4-ethylenedioxythiophene) polystyrene sulfonate (PEDOT:PSS), leading to the generation of high electro-chemo-mechanical performance of the corresponding composite electrodes. Finally, the developed ionic soft actuator based on the BS-COF-C electrode exhibits large bending strain (0.62%), excellent durability (90% retention for 6 hours under operation), and 2.7 times higher bending displacement than PEDOT:PSS under extremely low harmonic input of 0.5 V. This study reveals that the antagonistic functionality of heteroatom co-doped electrodes plays a crucial role in accelerating the actuation performance of ionic artificial muscles.

1. Introduction

Next-generation soft and wearable electronic products with flexible and bendable functionalities, which are compatible with dynamic changes of human body, will be integrated with real-time health-monitoring systems, active sport wear, and haptic feedback systems. Soft robots have been newly suggested and extensively investigated to replace conventional motor-based robots. Interestingly, both soft electronics and soft robotics will require soft and compliant actuating systems, which are key components to convert stimulus input signals into mechanical deformation and motion. Therefore, functionalized nanocarbon materials have received much attention as efficient electrodes for the exploration of electroactive soft actuators.[1–7] Recently, reduced graphene oxide paper,[3] heteroatom co-doped graphene,[4] hollow tubular graphene mesh,[8] and graphitic carbon nitride[9] have been investigated for the exploration of efficient ionic soft actuators. Further, hierarchical porous nitrogen-doped carbons, owing to their high specific surface area (SSA) and impressive electrical conductivity and electrochemical activity, have recently been used as electrodes for ultrasensitive bio-inspired artificial muscles.[10] Recently, heteroatom co-doping in porous carbon is a growing avenue of research in the fields of supercapacitors and electrocatalysts.[11–16] However, to the best of authors' knowledge, co-doped porous carbon-based electrodes for exploration of ionic soft actuators have not carefully been investigated to date by considering both direct current (DC) and alternating current (AC) input patterns.

Covalent organic frameworks (COFs) have gained significant attention as a new type of crystalline porous materials, developed by polymerization of organic building blocks with desired functional groups.[17–24] With their high surface area, tunable compositions, and diverse structural topologies, they have been widely explored for catalysis, gas storage and separation, and proton conduction.[25–32] These materials are outstanding templates for

Prof. S. Roy, Dr. J. Kim, Prof. M. Kotal, Dr. R. Tabassian, Prof. I.-K. Oh
Creative Research Initiative Center for Functionally Antagonistic Nano-Engineering
Department of Mechanical Engineering
Korea Advanced Institute of Science and Technology (KAIST)
291 Daehak-ro, Yuseong-gu, Daejeon 34141, Republic of Korea
E-mail: ikoh@kaist.ac.kr
The ORCID identification number(s) for the author(s) of this article can be found under https://doi.org/10.1002/adfm.201900161.

Prof. S. Roy, Prof. M. Kotal
Department of Chemistry
Maharishi Markandeshwar Deemed to be University
Mullana (Ambala) 133207, Haryana, India
Prof. K. J. Kim
Department of Mechanical Engineering
University of Nevada
Las Vegas, 4505 Maryland Parkway, Las Vegas, NV 89154, USA

DOI: 10.1002/adfm.201900161

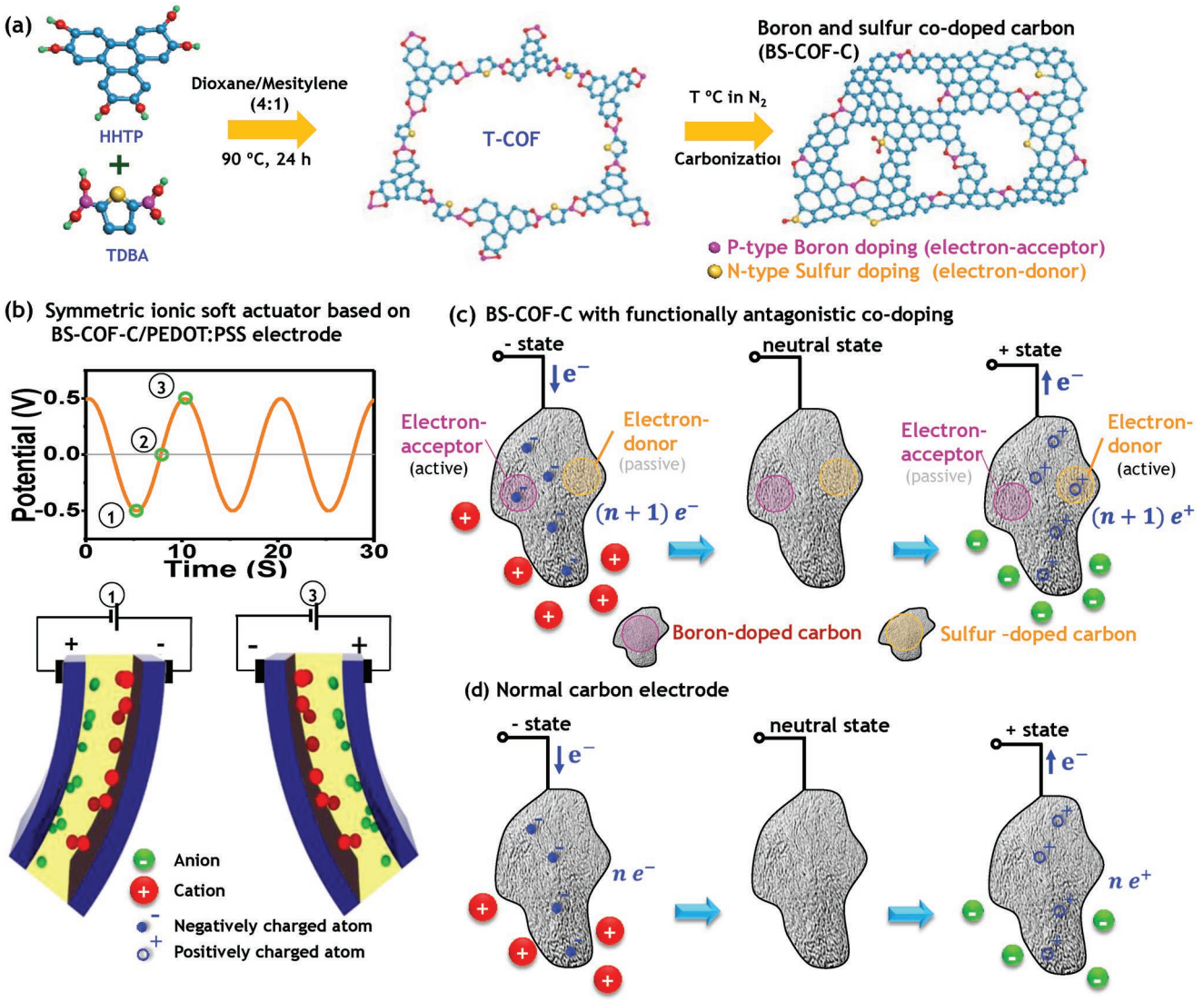

Figure 1. Schematic illustrations for the synthetic route of BS-COF-C and the actuation mechanism of the designed novel ionic actuator based on collectively exhaustive electrode with functionally antagonistic co-doping. a) Synthetic steps of BS-COF-C antagonistic electrode with hierarchical porosity by using T-COF as precursor via one-pot carbonization. b) Symmetric actuation mechanism of low-voltage-driven ionic actuator by using BS-COF-C antagonistic electrode demonstrating fast ion separation in the electrolyte membrane and large bending response. Effect of electron mobility and ionic interactions under electric field for c) BS-COF-C with functionally antagonistic co-doping and d) normal carbon electrode.

the preparation of heteroatom-doped porous carbons via pyrolysis process owing to their ordered porous structures, regular arrangement of diverse heteroatoms such as B, O, N, and S, and high concentrations of carbon species.[13,15,33] Notably, sulfur-doped carbon is more beneficial compared to nitrogen due to its linkage to the electron-rich aromatic sulfide, which offers more polarized surface under electric field leading to enhance dielectric constant of the electrolyte and assist the charge-transfer process.[16,34] Boron atom has one less electron than carbon, which introduces hole charge carrier while sulfur doping creates high electron density (compared to N) located at the surface of the carbon generating electron carrier, resulting in decreasing charge-transfer resistance and increasing conductivity.[16,35] The aforementioned properties are crucial for high-performance electro-ionic actuators. To the best of authors' knowledge, COF derived B and S co-doped hierarchical porous carbons (BS-COF-Cs) have not yet been explored as antagonistic electrodes for the development of highly bendable ionic artificial muscles. Boron and sulfur co-doping in porous carbons can be simultaneously designed to serve as electron acceptors and electron donors when they are used as electrodes in actuators.

In this study, a thiophene-based boronate-linked covalent organic framework (T-COF) is introduced as a precursor for the first time to synthesize BS-COF-C materials, through the direct pyrolysis process, as shown in **Figure 1**a. Additionally, high-performance electroactive artificial muscles were developed using T-COF-derived porous graphitic structured BS-COF-C electrodes. Such BS-COF-Cs are highly desirable to demonstrate promising electrochemical performances in both aqueous and nonaqueous electrolytes, as well as fast charge-transfer

responses, owing to their large specific surface area, abundant micro and mesoporosity, and lower charge-transfer resistance that stems from antagonistic heteroatom co-doping (B/S) in the graphitic carbon matrix. Most importantly, under harmonic inputs with AC signals, the two top and bottom electrodes in the electroactive ionic soft actuator will experience repeated changes between anode and cathode as shown in Figure 1b–d. Therefore, a collectively exhaustive co-doped electrode having both electron-donor (n-doped) and electron-acceptor (p-doped) components in functionally antagonistic co-doping arrangement will be very efficient in electroactive ionic soft actuating systems under harmonic inputs, as well as DC inputs. For the sake of comparison, B-COF-C electrode derived from COF-5 through pyrolysis was further introduced. A conductive polymer, poly(3,4 ethylenedioxythiophene) polystyrene sulfonate (PEDOT:PSS), was used as binder for BS-COF-Cs or B-COF-C to design flexible composite electrode (BS-COF-Cs/PEDOT:PSS or B-COF-C/PEDOT:PSS) with significant capacity and conductivity. Finally, the ionic-type actuator was fabricated by depositing the flexible composite electrodes on either side of ionic liquid embedded Nafion membrane. The designed actuator based on BS-COF- Cs/PEDOT:PSS electrode showed high charge storage and transfer abilities, along with promising electromechanical performances, including large specific capacitance (389 F g^{-1}) and ultrafast actuation response (large bending deformation of 8.60 mm under low input voltage ±0.5 V), which significantly outperformed the B-COF-C/PEDOT:PSS electrode-based actuator. As boron atom has one-electron deficiency compared to carbon, hole charge carrier is generated in BS-COF-C electrode, while sulfur creates an electron carrier owing to its high electron density. Therefore, the antagonistic functionality of the BS-COF-C electrode assists charge-transfer rate of the designed BS-COF-C/PEDOT:PSS flexible electrode under electric field, leading to fast charge separation in the developed ionic actuator. To further understand the collectively exhaustive behavior of the designed electrode, an asymmetric ionic actuator was developed using BS-COF-C900 and B-COF-C900 electrodes. Notably, the bending responses of the symmetric ionic actuator under varying ultralow voltage inputs are significantly higher than those of the asymmetric ionic actuator, owing to the synergistic effects of electron donor and electron acceptor, high ion-accessible surface area, and high charge storage ability of the BS-COF-C900 electrode compared to those characteristics of the B-COF-C900 electrode. To the best of our knowledge, T-COF-derived BS-COF-C materials with tunable porosity and heteroatom co-doping have not yet been employed as electrodes for highly efficient ionic actuators.

2. Results and Discussions

2.1. Synthesis and Characterization of T-COF and BS-COF-Cs

The synthesis of T-COF was carried out at high yield by condensation reaction of 2,3,6,7,10,11-hexahydroxytriphenylene with 2,5-thiophenediboronic acid under modified reflux conditions (Figure 1a).[36,37] The formation of T-COF and COF-5 was ensured through the solid-state ^{13}C CP-MAS nuclear magnetic resonance, Fourier transform infrared spectra, and powder X-ray diffraction (PXRD) analysis (Figures S1–S3, Supporting Information). The higher Brunauer–Emmett–Teller (BET) surface area with mesoporosity (Figure S4, Supporting Information) makes the T-COF template a promising carbon source to synthesize BS-COF-C electrodes (BS-COF-C700 and BS-COF-C900) through one-pot pyrolysis at 700 and 900 °C. Also, B-COF-C900 electrode was obtained via one-pot pyrolysis of COF-5 template at 900 °C. The morphology of T-COF and BS-COF-Cs as presented in **Figure 2**a–c using field emission scanning electron microscopy (FESEM) reveals layered sheet-like morphology with porous nature, although loose packing with more porous features was detected in BS-COF-Cs. Additionally, morphology analyses of COF-5 and B-COF-C900 also depict layered sheet structures (Figure S5, Supporting Information). Scanning transmission electron microscopy (STEM) further confirms the formation of layered sheet-like structure for BS-COF-C900 (Figure 2d). To ensure the co-doping of boron and sulfur in the carbon matrix of BS-COF-C900, elemental mapping was conducted using STEM (inset of Figure 2d), which revealed that boron and sulfur atoms are uniformly distributed throughout the BS-COF-C900 network. High-resolution TEM (HRTEM) imaging of BS-COF-C900 implies very prominent graphitic structure with layer spacing of around 0.34 nm, marginally lesser than BS-COF-C700 (layer spacing ≈0.36 nm), as depicted in Figure 2e,f. These findings indicate the higher degree of graphitization of BS-COF-C900 than BS-COF-C700, which agrees with PXRD and Raman results. Such ordered graphitic structure is highly beneficial for enhancing the electrical conductivity of electrodes.[10,38] The selected area electron diffraction (SAED) pattern reveals two diffraction rings attributed to (002) and (101) peaks, suggesting the graphitic structure with a partially amorphous character (Figure 2f).

Structural characterizations of BS-COF-Cs and B-COF-C by employing PXRD, Raman spectra, N_2 adsorption–desorption isotherms, and pore size distributions (PSDs) further offer additional evidence for the formation of graphitic structures and hierarchical porosity of the electrodes as elaborately discussed in Figures S6 and S7 (Supporting Information). Comparatively broadened peak at ≈23.5° with increased intensity at 43.5° in PXRD and relatively lower intensity ratio (≈0.86) of the D to G band (I_D/I_G) as well as more prominent broad peak at about 2650 cm^{-1} in Raman Spectra for BS-COF-C900 than BS-COF-C700 and B-COF-C900 further reaffirm the generation of higher degree of graphitic structure in BS-COF-C900 than other electrodes. Moreover, the larger BET surface area (SSA) (720.57 m^2 g^{-1}), enhanced pore volume (0.39 cm^3 gm^{-1}) associated with rapid nitrogen uptake in very low-pressure region ($P/P_0 < 0.1$), and increased PSD peak intensities centered at 0.97, 1.19, 1.33, 2.69, 9.38, and 43.35 nm for BS-COF-C900 compared to other electrodes imply the presence of hierarchical porosity with more abundance of micro and mesopores in BS-COF-C900. The observed higher degree of graphitization, larger SSA, and pore volume together with well-interconnected porous structure of BS-COF-C900 are highly beneficial to improve ion storage and transfer capacity of the electrode, which are the critical prerequisites for exhibiting remarkable electrochemical performance. Thus, BS-COF-C900 is anticipated to be an efficient candidate for electrode toward

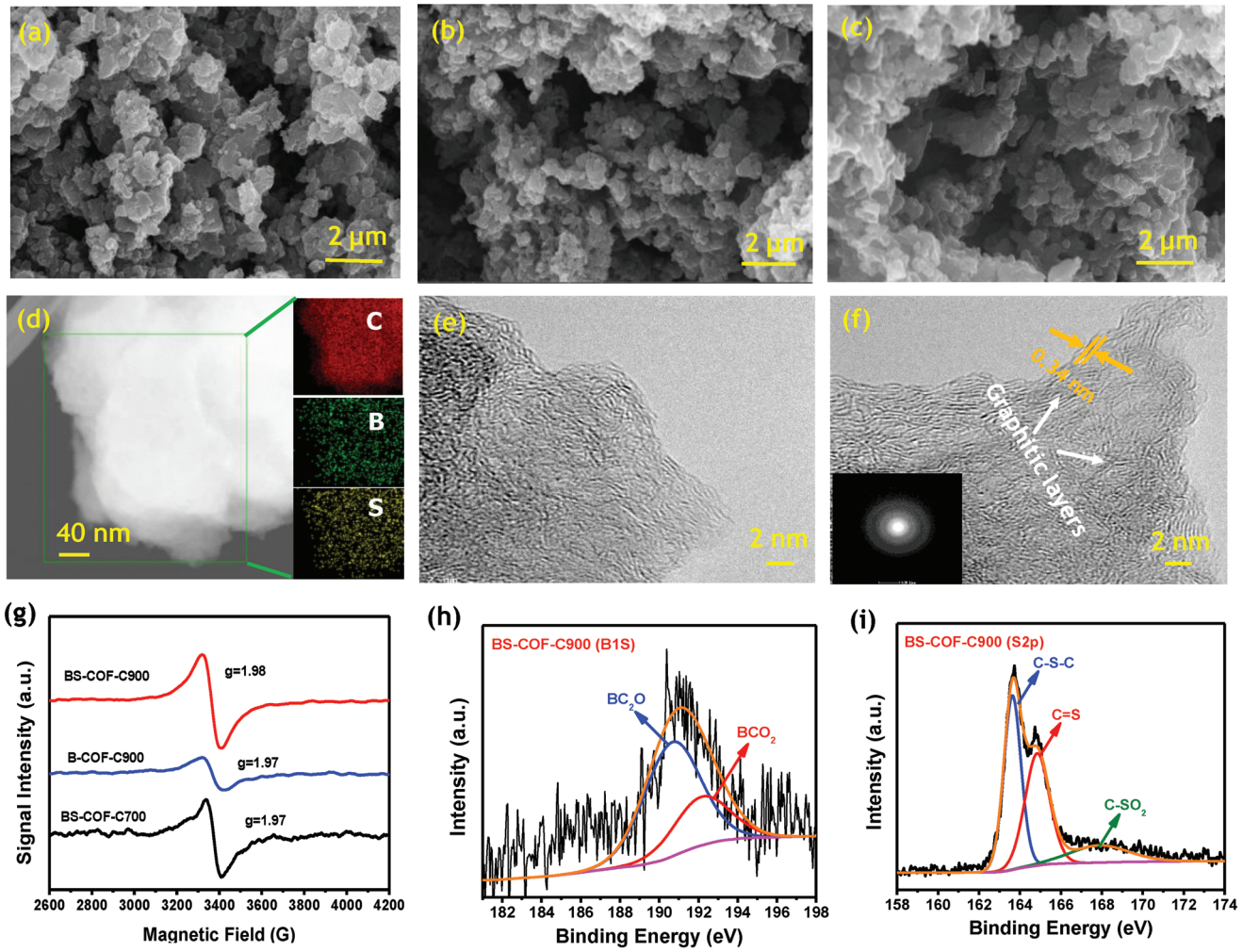

Figure 2. Morphological characterizations of the as-synthesized T-COF and BS-COF-C electrode materials. FESEM images of a) T-COF, b) BS-COF-C700, and c) BS-COF-C900. d) STEM image of BS-COF-C90 and the inset shows its corresponding carbon, boron, and sulfur elemental mapping images. HRTEM images of e) BS-COF-C700 and f) BS-COF-C 900. The inset is its corresponding SAED pattern. g) EPR spectra of BS-COF-C700, BS-COF-C900, and B-COF-C900. High-resolution XPS spectra of h) B1s and i) S 2p for BS-COF-C900.

the exploration of highly efficient ionic artificial muscles. To investigate the antagonistic behavior that can be achieved by B and S co-doping in BS-COF-C900, electron paramagnetic resonance (EPR) spectra were recorded for BS-COF-Cs and B-COF-C at room temperature for identifying the generation of charge carriers with unpaired electrons (free radicals).[39] Figure 2g reveals that all the materials exhibit radical signals at around $g = 1.97–1.98$ in X-band EPR. Interestingly, the intensity of the sharp radical signal is significantly higher for BS-COF-C900 than for BS-COF-C700 and B-COF-C900, confirming the effective charge transfer in BS-COF-C900. Moreover, the binding states and quantitative elemental compositions of BS-COF-Cs and B-COF-C were studied by X-ray photoelectron spectroscopy (XPS). The successful co-doping of B and S atoms into graphitic carbon frameworks of BS-COF-Cs was confirmed by the XPS survey spectra (Figure S8, Supporting Information). The elemental composition data of all the materials from XPS are presented in Table S1 (Supporting Information). The deconvoluted B1s spectra for BS-COF-Cs indicate the existence of two peaks at 190.8 eV (BC_2O) and 192.6 eV (BCO_2) (Figure 2h; Figure S9a, Supporting Information). Further, the deconvoluted S2p spectra for BS-COF-C900 reveal the existence of three peaks at 163.6 eV (−C−S−C−), 164.9 eV (−C=S−), and 168.0 eV (−C−SO_2−), whereas BS-COF-C700 displays one additional peak at 165.7 eV (−C−SO−), along with three other similar peaks (Figure 2i; Figure S9b, Supporting Information).[40] On the contrary, the XPS survey spectrum for B-COF-C900 exhibits only B 1s peak (Figure S8, Supporting Information). The deconvoluted B 1s spectra for B-COF-C900 show the existence of two similar peaks at 190.8 eV (BC_2O) and 192.6 eV (BCO_2), as in the case of BS-COF-Cs (Figure S9c, Supporting Information). These observations confirm that boron and sulfur have been co-doped into the graphitic carbon frameworks of BS-COF-Cs successfully; this co-doping can synergistically improve the electrical and electrochemical responses of BS-COF-C-based electrodes.[16,41] Therefore, BS-COF-C-based electrodes can be highly advantageous toward the development of efficient ionic actuators.

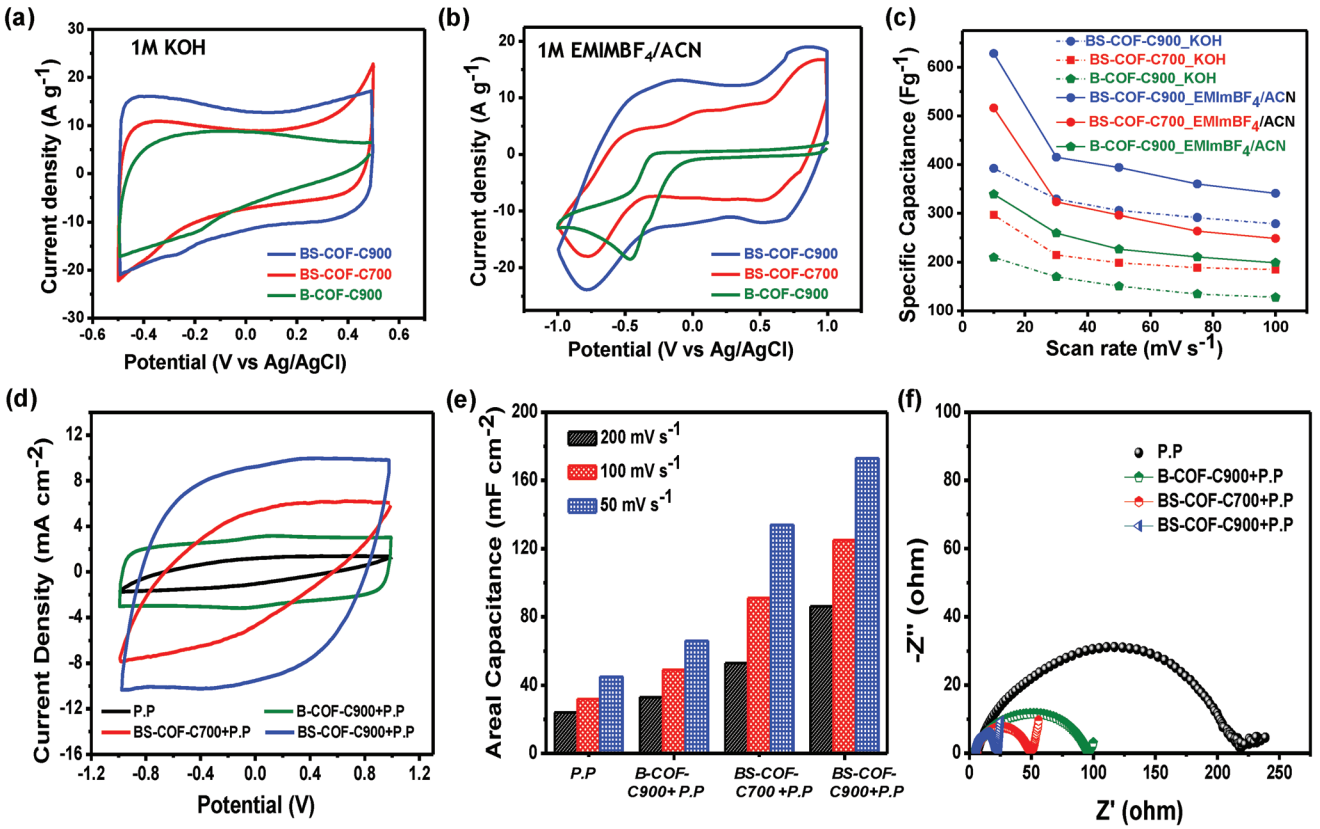

Figure 3. Electrochemical characterizations of synthesized electrodes and their composites based ionic actuators. Cyclic voltammetry (CV) analysis of BS-COF-C700, BS-COF-C900, and B-COF-C900 in a) 1.0 M KOH and b) 1.0 M EMIM-BF_4/CH_3CN electrolytes at a scan rate of 100 mV s^{-1}. c) The variation of specific capacitances with scan rates in both electrolytes. d) CV curves of the fabricated ionic actuators based on pristine P.P and its composite electrodes with BS-COF-C700, BS-COF-C900, and B-COF-C900 at a scan rate of 100 mV s^{-1}. e) Variation of areal capacitances with scan rates for the fabricated actuators. f) Nyquist plots of the actuators.

2.2. Electrochemical and Mechanical Properties of BS-COF-Cs Electrodes

As the charge-storage ability of the electrodes is a crucial factor in determining the actuation performance, cyclic voltammetry (CV) in both aqueous and nonaqueous electrolytes (1 M KOH and 1 M EMIM-BF_4/CH_3CN) was performed under various scan rates (10–100 mV s^{-1}) to determine the electrochemical behavior through a three-electrode system. The CV responses in the voltage range of +0.5 to −0.5 V at 100 mV s^{-1} for BS-COF-C700, BS-COF-C900, and B-COF-C900 in aqueous electrolyte imply the highest capacitance for BS-COF-C900 (**Figure 3**a). All the BS-COF-C-based electrodes exhibit rectangular-like CV curves without any prominent peaks from 10 to 100 mV s^{-1} revealing ideal electrical double-layer capacitor (EDLC) response and good rate capability (Figure S10a,b, Supporting Information). Conversely, CV curves of B-COF-C900-based electrode show distorted rectangular shapes at all mentioned scan rates (Figure S10c, Supporting Information). Integrating the CV curves of all electrodes yields the specific capacitances that are then plotted against scan rates (Figure 3c). Notably, BS-COF-C900 exhibited higher specific capacitance (389 F g^{-1}) at 10 mV s^{-1} than those of BS-COF-C700 (294 F g^{-1}) and B-COF-C900 (209 F g^{-1}) and even surpassed those of literatures reported heteroatom co-doped porous carbons.[11,14,38,41] The observed higher specific capacitance of BS-COF-C900 is attributed to its porous structure with higher abundance of mesopores and larger ion-accessible surface area than those of other electrodes; these characteristics promoted rapid electrolyte ion diffusion through the pores. Additionally, in BS-COF-C900, B and S co-doping led to generate many active sites, which facilitated more efficient binding interactions, resulting in the enhancement of the current density and charge transport rate.[4] As dry-type actuators would be explored with nonaqueous ionic liquid-EMImBF_4, analyses of the CV responses of the mentioned electrodes at 100 mV s^{-1} scan rate were also conducted in 1 M EMIM-BF_4/CH_3CN under −1.0 to +1.0 V potential range (Figure 3b). BS-COF-C-based electrodes were found to exhibit slight distortions in their rectangular CV curves, while the CV curve of B-COF-C900 showed distorted patterns. These results can be attributed to the significant ionic interactions of EMIM-BF_4 and boron and sulfur-based functional groups in the BS-COF-Cs (or boron-based functional groups in BCOF-C) electrodes.[4,9] BS-COF-C900 was found to exhibit the highest specific capacitance (341 F g^{-1} at 100 mV s^{-1}) over all the tested electrodes. Furthermore, analyses of CV curves of the electrodes under varying scan rates (10–100 mV s^{-1}) showed also unaltered shapes at all scan rates (Figure S11, Supporting

Information). Moreover, the specific capacitance variations with scan rate for all electrodes in nonaqueous electrolytes are presented in Figure 3c. Similar to the findings for the aqueous electrolyte, BS-COF-C900 possessed remarkably higher specific capacitances than those of the other two electrodes. Thus, the BS-COF-C900-based electrode is an ideal antagonistic electrode for the exploration of high-performance ionic artificial muscles. The charge storage capability of flexible electrodes by employing PEDOT:PSS (P.P) as binder was additionally investigated through performing CV at similar scan rates in the same ionic liquid (IL)-based electrolyte over the potential range of −1.0 to +1.0 V (Figures S12 and S13, Supporting Information). In particular, the plot of the volumetric capacitance with scan rate, shown in Figure S13b (Supporting Information), indicates that BS-COF-C900/P.P has volumetric capacitance of 12.097 F cm^{-3} at 10 mV s^{-1}, which is ≈4.7, 1.54, and 1.2 times more than neat P.P (2.57 F cm^{-3}), B-COF-C900/P.P (7.84 F cm^{-3}), and BS-COF-C700/P.P (10.0 F cm^{-3}), respectively. To further study the charge-transport responses of the electrodes, electrochemical impedance spectra were recorded, as depicted and explained in Figure S13c, Supporting Information. The lowest charge-transfer resistance (≈4.3 Ω) of BS-COF-C900/P.P assists fast electrolyte ion diffusion owing to the antagonistic functionality and synergistic effect of B and S. The electrical conductivities of the composites were further studied by four-probe method revealing that BS-COF-C900/P.P exhibited higher electrical conductivity (752 S cm^{-1}) than other electrodes owing to the modification of electronic structure (Table S2, Supporting Information). As electro-chemo-mechanical behavior of the electrodes plays a crucial role in ionic actuation, stress–strain behavior for the composites was explored (Figure S14 and Table S2, Supporting Information). Notably, BS-COF-C900/P.P exhibited the highest strength at failure (61 MPa) and tensile modulus (1664 MPa) due to strong interfacial interaction of B and S-based functional groups with P.P. To understand the obtained bending responses of fabricated actuators made of EMIM-BF_4-embedded Nafion membrane sandwiched by the composite electrodes, the charge accumulation ability and ionic mobility of the actuators were explored (Figure 3d–f). The almost rectangular CV patterns of the actuators at 100 mV s^{-1}, as displayed in Figure 3d, imply that all the actuators exhibit EDLC behavior. However, the area under the CV curve is highest for the BS-COF-C900/P.P-based actuator compared to other actuators. Furthermore, the areal capacitance variation with scan rate, shown in Figure 3e, reveals that, at all scan rates (50–200 mV s^{-1}), the BS-COF-C900/P.P-based actuator exhibited highest areal capacitances over other three actuators. More importantly, at 100 mV s^{-1}, BS-COF-C900/P.P-based actuator demonstrated capacitive flux of 125 F cm^{-2}, which retained the rate capability even at 200 mV s^{-1} (86 F cm^{-2}). The excellent charge storage ability of this actuator is due to the hierarchical porosity, large specific surface area, and antagonistic functionality of BS-COF-C900, which not only facilitates rapid ion flow via the electrode–electrolyte surface, but also promotes efficient binding interaction with EMIM-BF_4 of the ion-exchange membrane.[4,10] Additionally, the ion mobility responses of the actuators were investigated by high-frequency intercept; the real impedance axis in the Nyquist plots indicates that this actuator has the smallest charge-transfer resistance (≈24 Ω) over other actuators (Figure 3f). The results further reaffirm that the antagonistic behavior of BS-COF-C900 and significant interfacial interaction of BS-COF-C900/P.P with EMIM-BF_4 and-SO_3H of Nafion assist the ionic conductivity of the corresponding actuator. Therefore, the electrochemical properties of the electrodes are preserved despite combining with the ion exchangeable Nafion-EMIM-BF_4 membrane.

2.3. Symmetric and Asymmetric Actuation Performance of BS-COF-Cs-Based Soft Ionic Actuators

Using a laser sensor, the actuation responses of the fabricated dry-type ionic soft actuators were measured using different oscillation input voltages and frequencies to examine their bending performances. The dynamic bending displacement performances of the four different designed ionic actuators corresponding to sine waves with ultralow input potential of ±0.5 V and low excitation frequency of 0.1 Hz are presented in **Figure 4**a. As evident, BS-COF-C900/P.P shows exceptional bending displacement of about 8.60 mm, which was 2.70 times more than P.P-based actuator (≈3.18 mm) and surpassed that of BS-COF-C700/P.P (≈6.82 mm); it was even 1.49 times more than B-COF-C900/P.P-based actuator (≈5.74 mm). Remarkably, the bending response of the designed BS-COF-C900/P.P-based actuator is more than graphene-based actuators and even polymer organic framework derived carbon-based ionic actuators;[3,4,8,10,42] this excellent performance is due to the presence of a hierarchical micromesoporous network, higher degree of graphitization, and antagonistic functionality of the corresponding electrode. Moreover, boron atom contains one less electron compared to carbon, offering hole charge carrier, while sulfur doping creates high electron density at the surface of carbon, generating electron carrier and leading to reduce charge-transfer resistance of the designed flexible electrode. Thus, compared to the other electrodes, under electric input, more cations can hypothetically surround the cathode surface of BS-COF-C900/P.P, leading to faster separation of anions in the ionic liquid embedded Nafion membrane via electrostatic forces toward the anode side. The effects of different ultralow input voltages (±0.1 to ±0.5 V) on the bending displacements of the three designed actuators, along with the pristine P.P-based actuators, were further studied for 10 s under sine wave at 0.1 Hz (Figure 4b). It is observed that the tip displacements for all the ionic actuators increased linearly with sinusoidal potential inputs. Importantly, at all ultralow driven potentials, BS-COF-C900/P.P electrode-based actuator outperformed over all the other designed ionic actuators owing to the higher electrical conductivity, porous network, and higher capacitance of the electrode. Especially, under ±0.1 V potential input, it showed bending movement of about 2 mm, 3.4 times more than neat P.P-based actuator. This finding suggests that BS-COF-C900/P.P electrode-based actuator can perform effectively even at ultralow voltage input. Furthermore, influence of various ultralow input voltages on the bending responses and bending strains of the four designed ionic actuators is presented in Figure 4c. Detailed calculation of the bending strain under electrical input for the ionic actuators is described in the Experimental Section. As expected, compared to the other ionic actuators in this work and

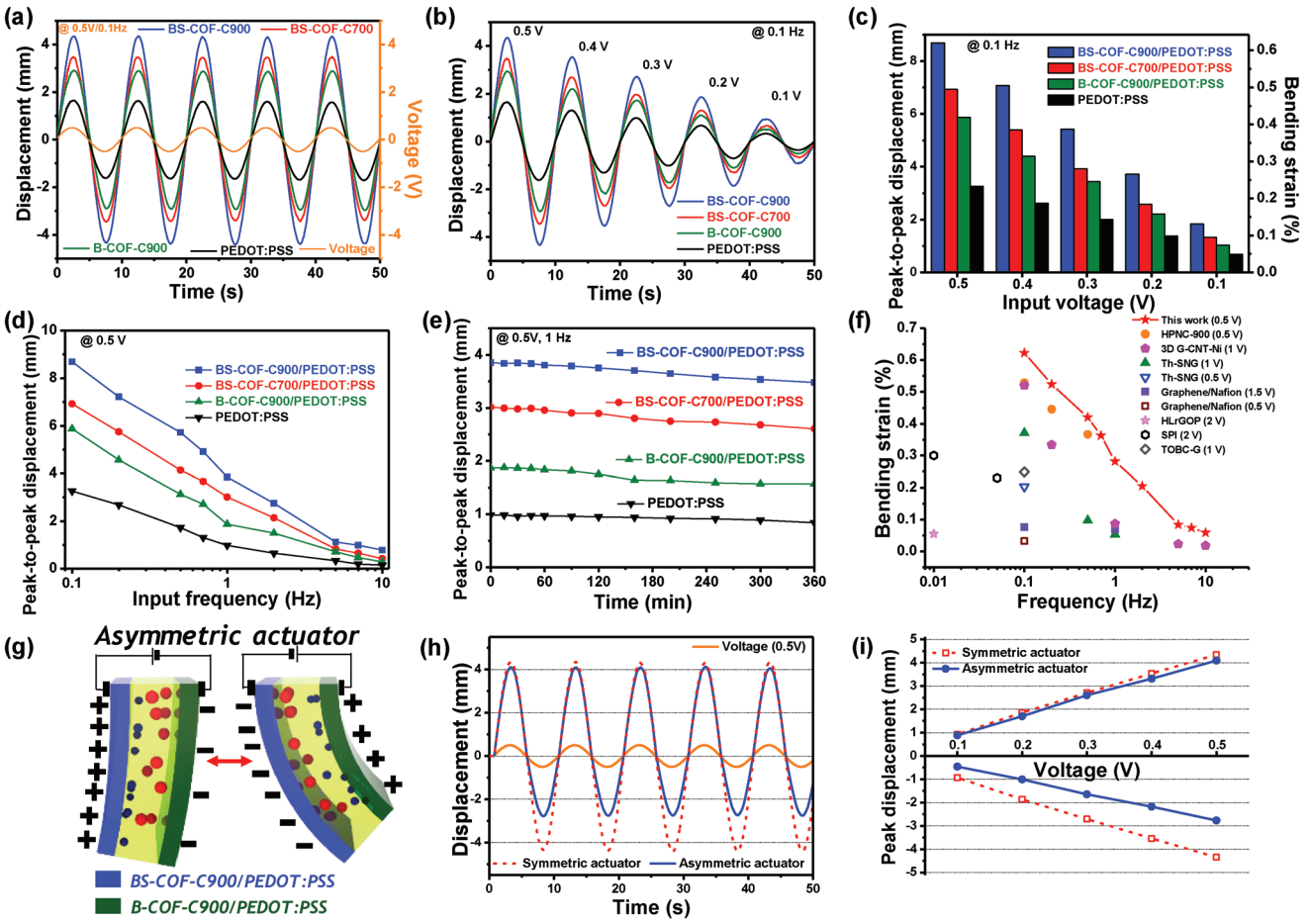

Figure 4. Actuation performances of fabricated symmetric and asymmetric actuators. a) Peak-to-peak displacements of the actuators under ±0.5 V sine wave input voltage at 0.1 Hz. b) Bending responses of the actuators under varying sine wave input voltages (0.1–0.5 V) at 0.1 Hz. c) Variation of peak-to-peak displacements and bending strains with different input voltages (0.1–0.5 V) at 0.1 Hz. d) Peak-to-peak displacements of the actuators as a function of applied frequency at ±0.5 V sine wave input voltage. e) Time-dependent displacements of the actuators under excitation of 0.5 V and 1 Hz. f) Comparison of bending strain–frequency curve of the designed actuator with the reported soft ionic actuators dealing with low-voltage operation. g) Schematic illustrations of asymmetric actuation mechanism of the asymmetric ionic actuator consisting of one side BS-COF-C900/P.P and other side B-COF-C900/P.P electrodes. h) Bending responses of the symmetric ionic actuator of BS-COF-C-900/P.P and its asymmetric ionic actuator with B-COF-900/P.P under sinusoidal input voltage of ±0.5 V, 0.1 Hz. i) Variation of peak-to-peak displacements of symmetric actuator (BS-COF-C900/Nafion/BS-COF-C900) and asymmetric actuator (BS-COF-C900/Nafion/B-COF-C900) at different input voltages (0.1–0.5 V) with excitation frequency of 0.1 Hz.

reported in the literature, the developed BS-COF-C900/P.P-based actuator exhibited maximum bending strain under all ultralow input voltages.[3,4,8,10,42] Furthermore, in order to compare the electromechanical performance of our designed ionic actuator with other electroactive polymers and similar actuator systems, the comparative representation with different electrodes and ionic membranes is presented in Table S3 (Supporting Information). The comparative study noticeably reveals that our designed ionic actuator based on the antagonistic electrode demonstrated excellent bending strain compared to other reported actuators even under the ultralow input voltage of 0.5 V. In particular, at ±0.5 V and 0.1 Hz, BS-COF-C900/P.P's calculated bending strain was found to be about 0.62%, almost 2.8 times more than neat P.P-based actuator. Additionally, under sinusoidal input of 0.5 V and a frequency window of 0.1 Hz to 10 Hz, the actuation performances of the designed actuators were examined, with the results being displayed in Figure 4d. With increasing excitation frequency, the peak-to-peak displacement gradually dropped for all the ionic actuators because the accessible time for ion diffusion was decreased. The BS-COF-C900/P.P electrode-based ionic actuator demonstrated maximum bending displacement for all excitation frequencies, benefitting from the synergistic effect of B and S co-doping with their antagonistic functionality, high electrical conductivity, the electrochemical activity and porous network in BS-COF-C900, and high mechanical resiliency through strong interaction of BS-COF-C900 with P.P, which results in enhanced charge inoculation and charge transport ability in P.P, expediting ion separation in the Nafion-EMImBF$_4$ membrane. To investigate the sustainability performance in air, durability tests were carried out by recording the bending responses for 6 h while employing sinusoidal input voltage of ±0.5 V and 1 Hz frequency (Figure 4e). It is noted that the designed BS-COF-C900/P.P electrode-based ionic actuator retained about 90% of its initial bending displacement even after 6 h, indicating its remarkable stability in air. The calculated

bending strain of the designed BS-COF-C900/P.P-based ionic actuator under different input frequencies, as depicted in Figure 4f, outperformed other reported ionic actuators dealing with low-voltage operations.[2–4,10,43,44] The peak-to-peak displacements of the actuators were also evaluated by employing square wave potential input of ±0.4 V and 0.1 Hz excitation frequency (Figure S15, Supporting Information). Similar to the findings for sinusoidal output response, all the ionic actuators demonstrated similar trends of bending responses. We also obtained the cross-sectional FESEM image of the tested ionic actuator to verify the homogeneous coating of the electrodes on the electrolyte membrane (Figure S16, Supporting Information). It is found that the designed composite electrodes were uniformly coated on the Nafion-IL membrane without any delamination along the boundary of the two electrode layers, further enhancing the actuation performance as well as the noteworthy durability. Furthermore, to understand the antagonistic functionality of the designed electrode, an asymmetric ionic actuator consisting of one side of BS-COF-C900/P.P and another side of B-COF-C900/P.P electrodes was fabricated and studied to determine its bending response under different ultralow input voltages. Figure 4g presents schematic illustrations of the mechanism for the different bending responses of the designed asymmetric ionic actuators when connected reversely with positive and negative electrodes. When the BS-COF-C900/P.P electrode was connected to the anode side and the B-COF-C900/P.P was connected to the cathode side, more anions hypothetically accumulated near the anode side; this can be compared to the accumulation of larger size cations near the cathode side owing to the synergistic effect of B and S co-doping and the relatively larger surface area, which resulted in slight bending toward the anode side. On the contrary, when BS-COF-C900/P.P electrode connected with cathode side, more cations were hypothetically surrounded near the cathode side compared to the anions near anode side, leading to large bending toward the anode side. Figure 4h depicts the dynamic bending responses of the symmetric actuators of BS-COF-C900/P.P electrode and its asymmetric actuator. It is observed that, for an asymmetric actuator under sinusoidal input voltage of ±0.5 V, B-COF-C900/P.P exhibited relatively less bending displacement than BS-COF-C900/P.P. Additionally, the bending responses of both symmetric and asymmetric actuators under different ultralow potential inputs (±0.1 to ±0.5 V) are shown in Figure 4i and Figure S17 (Supporting Information). Under all input voltages, owing to the greater accumulation of ions near the BS-COF-C900 side, comparatively less bending displacement occurred at the B-COF-C900 electrode side compared to the BS-COF-C900 side, further satisfying the importance of the use of antagonistic electrode for ionic artificial muscle. After analyzing the performance of suggested electrode, the as-prepared actuator was used to make a grapple robot (**Figure 5**). For this aim, six actuator strips were cut into

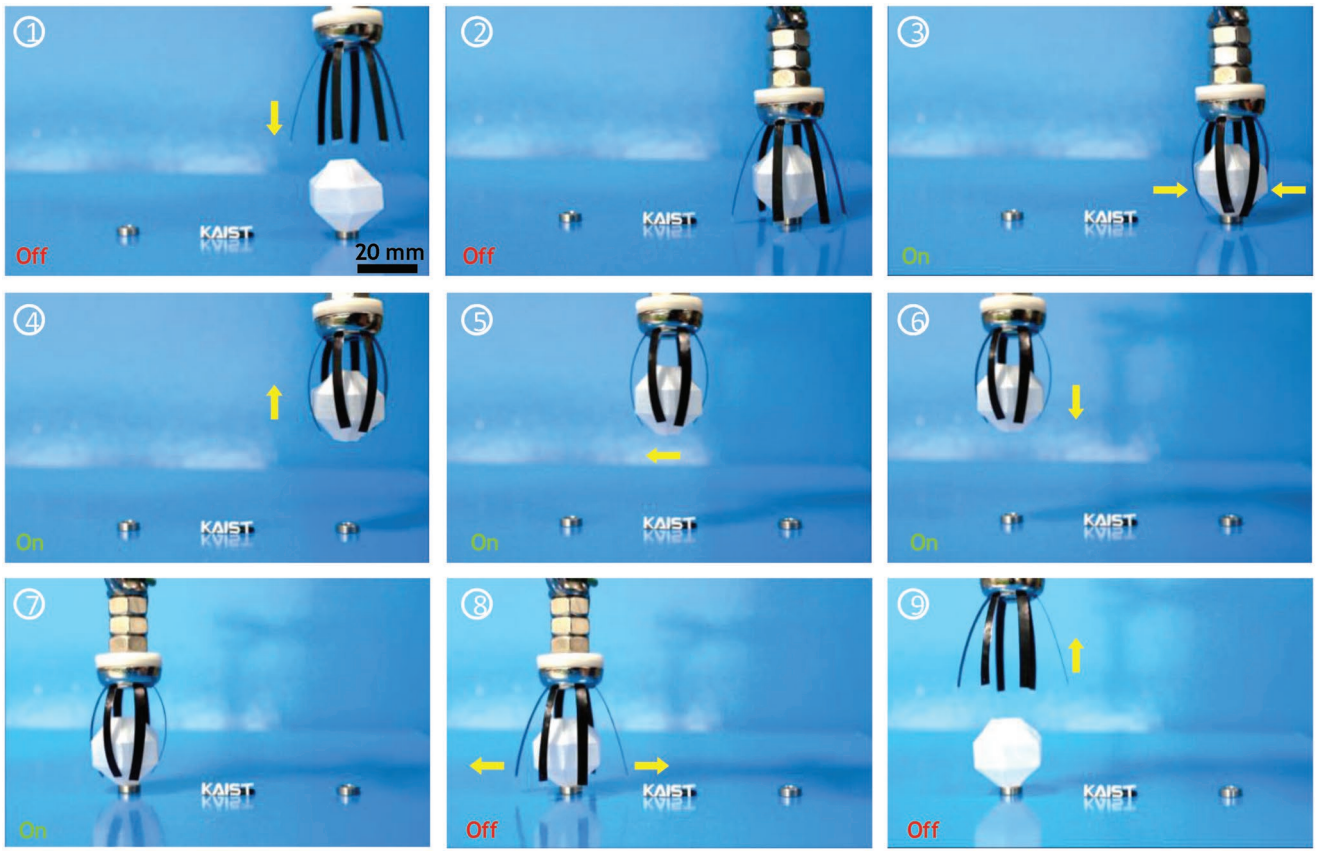

Figure 5. Operation of grapple robot consisting of six symmetric ionic actuators arms based on BS-COF-C-900/P.P electrodes by input voltage of 2.5 V. The weight of the relocated paper-based object is 55 mg.

40 mm × 5 mm pieces and clamped at the ends. The clamping points were oriented 45° with respect to vertical direction. All electrodes were linked in parallel to the power supply. The grapple was positioned on top of the object and approached it. By applying input voltage of 2.5 V, the arms were actuated and grabbed the object. The robot moved to the target position to relocate the object. When the object reached the target position, the voltage was removed to release the object. In this experiment, the weight of the relocated object was 55 mg, which is around nine times greater than our previous report.[8] This prototype shows the capability of the newly designed actuator for practical robotic applications.

3. Conclusion

In summary, by introducing collectively exhaustive boron and sulfur co-doped porous carbon electrodes (BS-COF-Cs), derived from T-COF, we were able to explore ultralow voltage driven ionic soft actuators. We further designed an asymmetric ionic actuator by employing B-COF-C900 along with BS-COF-C900 electrodes. Interestingly, the overall bending response of the symmetric ionic actuator is significantly higher than that of the asymmetric ionic actuator because of the electron donor and acceptor antagonistic functionality, high surface area, high degree of graphitization, and high specific capacitance of BS-COF-C900 compared to those characteristics of the B-COF-C900 electrode. Based on this highly competent actuation mechanism, the as-designed BS-COF-C900 actuator exhibits intriguing actuation performance, including a large bending response of 8.60 mm and bending strain of 0.62%, wide frequency response (up to 10 Hz), and 6 h durability (retention about 90% of initial bending displacement at 1 Hz) under ±0.5 V. Moreover, the fast and visible motion of the grapple robot model reflected its immense potential toward the exploration of biomimetic devices. Finally, we anticipate that the newly developed functionally antagonistic electrode-based actuator will have immense potential in the fields of soft artificial muscles and biomedical microdevices.

4. Experimental Section

The detailed experimental process is available in the Supporting Information.

Supporting Information

Supporting Information is available from the Wiley Online Library or from the author.

Acknowledgements

This work was partially supported by the Creative Research Initiative Program (2015R1A3A2028975), funded by the National Research Foundation of Korea (NRF). K.J.K. acknowledges partial financial support from the US National Science Foundation (NSF), Partnerships for International Research and Education (PIRE) Program, Grant No. 1545857. Any opinions, findings, and conclusions or recommendations expressed in this material are those of the author(s) and do not necessarily reflect the views of the NSF.

Conflict of Interest

The authors declare no conflict of interest.

Keywords

antagonistic, artificial muscles, covalent organic framework, hierarchical porosity, supercapacitors, synergistic

Received: January 6, 2019
Revised: February 18, 2019
Published online: February 28, 2019

[1] S. E. Zhu, R. Shabani, J. Rho, Y. Kim, B. H. Hong, J. H. Ahn, H. J. Cho, *Nano Lett.* **2011**, *11*, 977.
[2] S. S. Kim, J. H. Jeon, H. I. Kim, C. D. Kee, I. K. Oh, *Adv. Funct. Mater.* **2015**, *25*, 3560.
[3] J. Kim, J. H. Jeon, J. J. Kim, H. Lim, I. K. Oh, *ACS Nano* **2014**, *8*, 2986.
[4] M. Kotal, J. Kim, K. J. Kim, I. K. Oh, *Adv. Mater.* **2016**, *28*, 1610.
[5] T. Fukushima, K. Asaka, A. Kosaka, T. Aida, *Angew. Chem., Int. Ed.* **2005**, *44*, 2410.
[6] L. Lu, W. Chen, *Adv. Mater.* **2010**, *22*, 3745.
[7] L. Lu, J. Liu, Y. Hu, Y. Zhang, H. Randriamahazaka, W. Chen, *Adv. Mater.* **2012**, *24*, 4317.
[8] R. Tabassian, J. Kim, V. H. Nguyen, M. Kotal, I. K. Oh, *Adv. Funct. Mater.* **2018**, *28*, 1705714.
[9] G. Wu, Y. Hu, Y. Liu, J. Zhao, X. Chen, V. Whoehling, C. Plesse, G. T. M. Nguyen, F. Vidal, W. Chen, *Nat. Commun.* **2015**, *6*, 7258.
[10] S. Roy, J. Kim, M. Kotal, K. J. Kim, I. K. Oh, *Adv. Sci.* **2017**, *4*, 1700410.
[11] Y. Li, G. Wang, T. Wei, Z. Fan, P. Yan, *Nano Energy* **2016**, *19*, 165.
[12] J. Zhang, Z. Yang, J. Qiu, H. W. Lee, *J. Mater. Chem. A* **2016**, *4*, 5802.
[13] C. You, X. Jiang, X. Wang, Y. Hua, C. Wang, Q. Lin, S. Liao, *ACS Appl. Energy Mater.* **2018**, *1*, 161.
[14] Y. Zhou, R. Ma, S. L. Candelaria, J. Wang, Q. Liu, E. Uchaker, P. Li, Y. Chen, G. Cao, *J. Power Sources* **2016**, *314*, 39.
[15] L. Li, L. Li, C. Cui, H. Fan, R. Wang, *ChemSusChem* **2017**, *10*, 4921.
[16] C. P. Yang, Y. X. Yin, H. Ye, K. C. Jiang, J. Zhang, Y. G. Guo, *ACS Appl. Mater. Interfaces* **2014**, *6*, 8789.
[17] A. P. Côté, A. I. Benin, N. W. Ockwig, M. O'Keeffe, A. J. Matzger, O. M. Yaghi, *Science* **2005**, *310*, 1166.
[18] H. Furukawa, O. M. Yaghi, *J. Am. Chem. Soc.* **2009**, *131*, 8875.
[19] X. Feng, X. S. Ding, D. Jiang, *Chem. Soc. Rev.* **2012**, *41*, 6010.
[20] C. J. Doonan, D. J. Tranchemontagne, T. G. Glover, J. R. Hunt, O. M. Yaghi, *Nat. Chem.* **2010**, *2*, 235.
[21] S. Chandra, S. Kandambeth, B. P. Biswal, B. Lukose, S. M. Kunjir, M. Chaudhary, R. Babarao, T. Heine, R. Banerjee, *J. Am. Chem. Soc.* **2013**, *135*, 17853.
[22] Q. Fang, Z. Zhuang, S. Gu, R. B. Kaspar, J. Zheng, J. Wang, S. Qiu, Y. Yan, *Nat. Commun.* **2014**, *5*, 4503.
[23] A. Nagai, Z. Guo, X. Feng, S. Jin, X. Chen, X. Ding, D. Jiang, *Nat. Commun.* **2011**, *2*, 536.
[24] H. Xu, X. Chen, J. Gao, J. Lin, M. Addicoat, S. Irle, D. Jiang, *Chem. Commun.* **2014**, *50*, 1292.
[25] Y. Zeng, R. Zou, Y. Zhao, *Adv. Mater.* **2016**, *28*, 2855.

[26] S. Chandra, T. Kundu, S. Kandambeth, R. BabaRao, Y. Marathe, S. M. Kunjir, R. Banerjee, *J. Am. Chem. Soc.* **2014**, *136*, 6570.
[27] V. S. Vyas, F. Haase, L. Stegbauer, G. Savasci, F. Podjaski, C. Ochsenfeld, B. V. Lotsch, *Nat. Commun.* **2015**, *6*, 8508.
[28] S. Y. Ding, J. Gao, Q. Wang, Y. Zhang, W. G. Song, C. Y. Su, W. Wang, *J. Am. Chem. Soc.* **2011**, *133*, 19816.
[29] Z. Li, T. He, L. Liu, W. Chen, M. Zhang, G. Wu, P. Chen, *Chem. Sci.* **2017**, *8*, 781.
[30] Q. Sun, B. Aguila, J. Perman, N. Nguyen, S. Ma, *J. Am. Chem. Soc.* **2016**, *138*, 15790.
[31] G. Lin, H. Ding, D. Yuan, B. Wang, C. Wang, *J. Am. Chem. Soc.* **2016**, *138*, 3302.
[32] N. Huang, L. Zhai, D. E. Coupry, M. A. Addicoat, K. Okushita, K. Nishimura, T. Heine, D. Jiang, *Nat. Commun.* **2016**, *7*, 12325.
[33] Q. Xu, Y. Tang, L. Zhai, Q. Chena, D. Jiang, *Chem. Commun.* **2017**, *53*, 11690.
[34] W. Deng, Y. Zhang, L. Yang, Y. Tan, M. Ma, Q. Xie, *RSC Adv.* **2015**, *5*, 13046.
[35] P. Babu, S. Mohanty, B. Naik, K. Parida, *ACS Appl. Energy Mater.* **2018**, *1*, 5936.
[36] G. H. V. Bertranda, V. K. Michaelis, T. C. Ong, R. G. Griffin, M. Dincă, *Proc. Natl. Acad. Sci. USA* **2013**, *110*, 4923.
[37] B. J. Smith, W. R. Dichtel, *J. Am. Chem. Soc.* **2014**, *136*, 8783.
[38] T. Wei, Q. Zhang, X. Wei, Y. Gao, H. Li, *Sci. Rep.* **2016**, *6*, 22646.
[39] H. Yan, J. Chen, K. Zhou, Y. Tang, *Adv. Energy Mater.* **2018**, *8*, 1703672.
[40] Y. Ito, W. Cong, T. Fujita, Z. Tang, M. Chen, *Angew. Chem.* **2015**, *127*, 2159.
[41] J. Hao, J. Wang, S. Qin, D. Liu, Y. Li, W. Lei, *J. Mater. Chem. A* **2018**, *6*, 8053.
[42] M. Kotal, J. Kim, R. Tabassian, S. Roy, V. H. Nguyen, N. Koratkar, I. K. Oh, *Adv. Funct. Mater.* **2018**, *28*, 1802464.
[43] R. K. Cheedarala, J. H. Jeon, C. D. Kee, I. K. Oh, *Adv. Funct. Mater.* **2014**, *24*, 6005.
[44] J. H. Jung, J. H. Jeon, V. Sridhar, I. K. Oh, *Carbon* **2011**, *49*, 1279.